Check for updates

Two-photon pumped forward, backward and random lasing in a stilbazolium dye nanocomposite solution containing LAPONITE® as a scattering center

Guang S. He,*[a,b] Sonal Gupta,[a,b] Richard A. Vaia, [c] Yogesh M. Joshi [d] and Paras N. Prasad [*a,b]

Multiphoton upconversion lasing in scattering gain media has attracted considerable attention in recent years. LAPONITE® is a scattering medium consisting of 2-D nano-discs that can be dispersed as a transparent solution in aqueous media and forms a gel at high concentration. In this paper, we demonstrate two-photon pumped upconversion regular lasing along forward and backward directions as well as random lasing along all other directions. The gain medium was a mixture of PRL-L5 dye solution in DMF with a water solution of LAPONITE® in which LAPONITE® nano-discs of 25–30 nm diameter may form large-size particles of several hundred nanometers due to electrostatic binding between the dye molecules and the LAPONITE® nano-discs, and therefore can produce more efficient scattering feedback for random lasing generation. Using 795 nm and 100 fs laser pulses as two-photon pump sources, we observed random lasing at around 500 nm, characterized by both spectral and temporal narrowing in all directions apart from the traditional (colinear forward/backward) lasing directions. The peak spectral intensity of random lasing is ~3.4 times higher than the normal fluorescence emission, but 10^5–10^6 times lower than the traditional forward lasing. This study shows the feasibility of generating both traditional forward/backward and random lasing in a moderately scattering gain medium for applications in diverse fields such as remote sensing, optical communications, and upconversion imaging.

1. Introduction

Multi-photon pumped lasing is an effective approach for generating frequency-upconversion coherent emission using near- and mid-IR laser radiation as pump sources.[1–14] This lasing technique has gained significant attention due to its applications in various fields such as biological imaging, remote sensing, LiDAR, and optical communications. Unlike traditional lasing, which relies on the optical cavity to govern amplification, random lasing belongs to a special class in which the amplification of emission is realized through optical feedback achieved by scattering.

*[a]Department of Chemistry, University at Buffalo, SUNY, New York 14260, USA.
E-mail: gshe@buffalo.edu, pnprasad@buffalo.edu*
[b]The Institute for Lasers, Photonics, and Biophotonics, University at Buffalo, SUNY, New York 14260, USA
[c]Materials and Manufacturing Directorate, Air Force Research Laboratories, Wright-Patterson Air Force Base, Dayton, OH 45433, USA
[d]Department of Chemical Engineering, Indian Institute of Technology Kanpur, Kanpur, 208016, India

In contrast to traditional (regular) lasing generated in optically transparent and neat gain media (gases, liquids, solids, fibers and waveguides), researchers can also generate stimulated emission in highly scattering and non-uniform gain media such as powders, colloidal particles, and dye solutions with suspended particles. In these cases, the observed stimulated emission exhibits spectral and temporal narrowing above a certain pump threshold, but no directionality.[15–21]

A wide range of nano-materials such as titania, silica, graphene, transition metal dichalcogenides, metal perovskites, *etc.* have been explored and employed in random lasing studies, where pump light is multiply scattered and the initial stimulated emission signals are amplified due to the scattering actions produced by the randomly distributed particles or domains. However, considering specifically nano-clay materials, only a few recent studies have reported this random lasing behavior. The unique properties of clay materials, including small particle sizes ranging from a few to hundreds of nanometers, large surface area, and cation exchange capacity, promote them as potential candidates to be scattering centers for random lasing.[22–26] For example, kaolinite nanoclay particles have been used as scatterers with rhodamine dye as a disordered gain medium for one-

photon excited random lasing.[27] Another example is that in which Pramanik *et al.* described halloysite nanotubes as light scatterers for one-photon pumped random lasing using rhodamine dye.[28] It is important to note that kaolinite, hydrous aluminum silicate, is 1 : 1 clay and halloysite belongs to the kaolinite family. LAPONITE®, on the other hand, is 2 : 1 smectite clay and is structurally very different from kaolinite.[29] Furthermore, the primary particle size of LAPONITE® is far smaller than that of other clay materials.[30,31] To our knowledge, no study has been reported using a general class of 2 : 1 smectite platelets, let alone LAPONITE® particles, as a disordered medium to achieve random lasing. In addition, no report of multiphoton lasing using clay materials has been stated.

This work extends our recent findings, where we observed significantly enhanced luminescence of a cationic stilbazolium dye in a solution containing LAPONITE®, that is due to the interaction between the dye molecules and the LAPONITE® nano-discs under the conditions of low dye concentration ($\leq$35 μM).[32] Here, we demonstrate that under two-photon pump conditions, both traditional and random lasing can be generated in an organic–inorganic disordered hybrid material (dye solution + LAPONITE® solution), in which the large clusters of LAPONITE® particles of 200–300 nm size act as effective scatterers caused by electrostatic binding between the dye molecules and the LAPONITE® nano-discs. Using 795 nm and 100 fs laser pulses, we conducted quantitative measurements of the spectral, temporal, and spatial properties of the lasing output. These measurements facilitate a deeper understanding and bridge the gap between random and traditional lasing.

2. Materials and methods

2.1 Preparation of LAPONITE® solution

The LAPONITE® XLG used in this study was procured from BYK Ltd. LAPONITE® is a synthetic clay that is widely used as a thickening and gelling agent and is commercially available in large quantities at low cost. A typical LAPONITE® nano-disc, with the formula $Na_{0.7}[(Si_8Mg_{5.5}Li_{0.3})O_{20}(OH)_4]$, has a diameter of 25–30 nm and a thickness of 1 nm.[28] Each LAPONITE® nano-disc consists of two tetrahedral silica layers sandwiching an octahedral layer of magnesia. Isomorphic substitution of some magnesium atoms by lithium creates a net negative charge across the nano-disc. This negative charge is compensated by sodium ions within the interlayer gallery between stacked nano-discs, making the overall structure of a LAPONITE® crystallite neutral. A LAPONITE® particle is an agglomeration composed of many of these crystallites. In water, a LAPONITE® crystallite swells and hydrated sodium ions dissociate from the surface of the nano-discs, leaving a net negative charge on the faces. Furthermore, when LAPONITE® is added to water having neutral pH, the pH increases to 9–10, suggesting protonation of the nano-disc edges making them positively charged.[28]

A stock solution of 0.75 wt% LAPONITE® was prepared by dissolving 75 mg of LAPONITE® in 10 mL of Milli Q water in a sealed vial by continuous stirring for 8–10 hours.

2.2 Preparation of L1 dye solution in DMF

A family of cationic stilbazolium dyes (labeled as PRL dyes) has been synthesized and reported in our previous studies, which are suitable for multiphoton pumped lasing purpose because of their superior solubility in polar solvents (such as DMSO, DMF, *etc.*), low pump threshold requirement because of high multiphoton absorption cross-section, and high lasing efficiency.[1,3] These dyes have the same molecular backbone but differ either in their electron donor or their electron acceptor moieties. In this study, we have chosen 4-[(*E*)-2-(4-methoxy-phenyl)ethenyl]-1-methylpyridinium iodide, PRL-L1 dye (labeled as L1 dye hereafter), as the two-photon pumped lasing dye because of its low lasing threshold requirement and high stability in solvent DMF or water. L1 dye can interact with the negatively charged nano-disc faces of LAPONITE® and may change the aggregation behavior of these nano-discs.

In this work, we prepared the L1 dye solution in DMF of 0.02 M concentration as the gain medium, in which we could easily generate two-photon pumped traditional lasing.

2.3 Preparation of the L1 dye–LAPONITE® hybrid

To achieve random lasing, we mixed the ~0.02 M L1 dye/DMF solution and 0.75 wt% LAPONITE®/water to obtain the L1 dye–LAPONITE® hybrid. The volume ratios of L1 dye/DMF and LAPONITE®/water were kept as 10 : 0.5, 10 : 1, and 10 : 2, respectively. This resulted in the formation of large-size LAPONITE® particles that play a crucial role as being more effective scattering centers in random lasing generation.

The dye concentration for this lasing study was kept at 0.02 M, and for complete exchange, a mass ratio of 5 : 1 (LAPONITE® to dye) is required. For the formulations examined, the amount of dye is approximately 50 times higher than LAPONITE®, which indicates that all exchangeable sites on LAPONITE® are occupied by the L1 dye (cation exchange capacity of LAPONITE® is 56.5 meq per 100 g) and excess dye remains in solution. At such a high L1 dye concentration, the surfaces of the nano-discs become fully neutralized by the positively charged dye molecules, leading to the stacking of nano-discs and the formation of larger particles in the predominately DMF solution as schematically shown in Fig. 1.

2.4 Characterization and transmission spectra

To determine the statistical distribution of the sizes of LAPONITE® particles suspended in the dye solution, a Malvern Zetasizer (ZSU3200) instrument was used for the dynamic light scattering (DLS) study at room temperature. For all DLS measurements, the samples were diluted ~400 times with DMF/water based on their actual concentration.

For scanning electron microscopy (SEM) analysis, films were drop cast on silicon substrates and dried in a vacuum. The SEM analysis employed a Hitachi SU70 scanning electron microscope. The samples were diluted 10 times with DMF based on their actual concentrations.

The transmission spectra of four 1 mm solution samples are shown in Fig. 2(a), indicating that all tested samples are
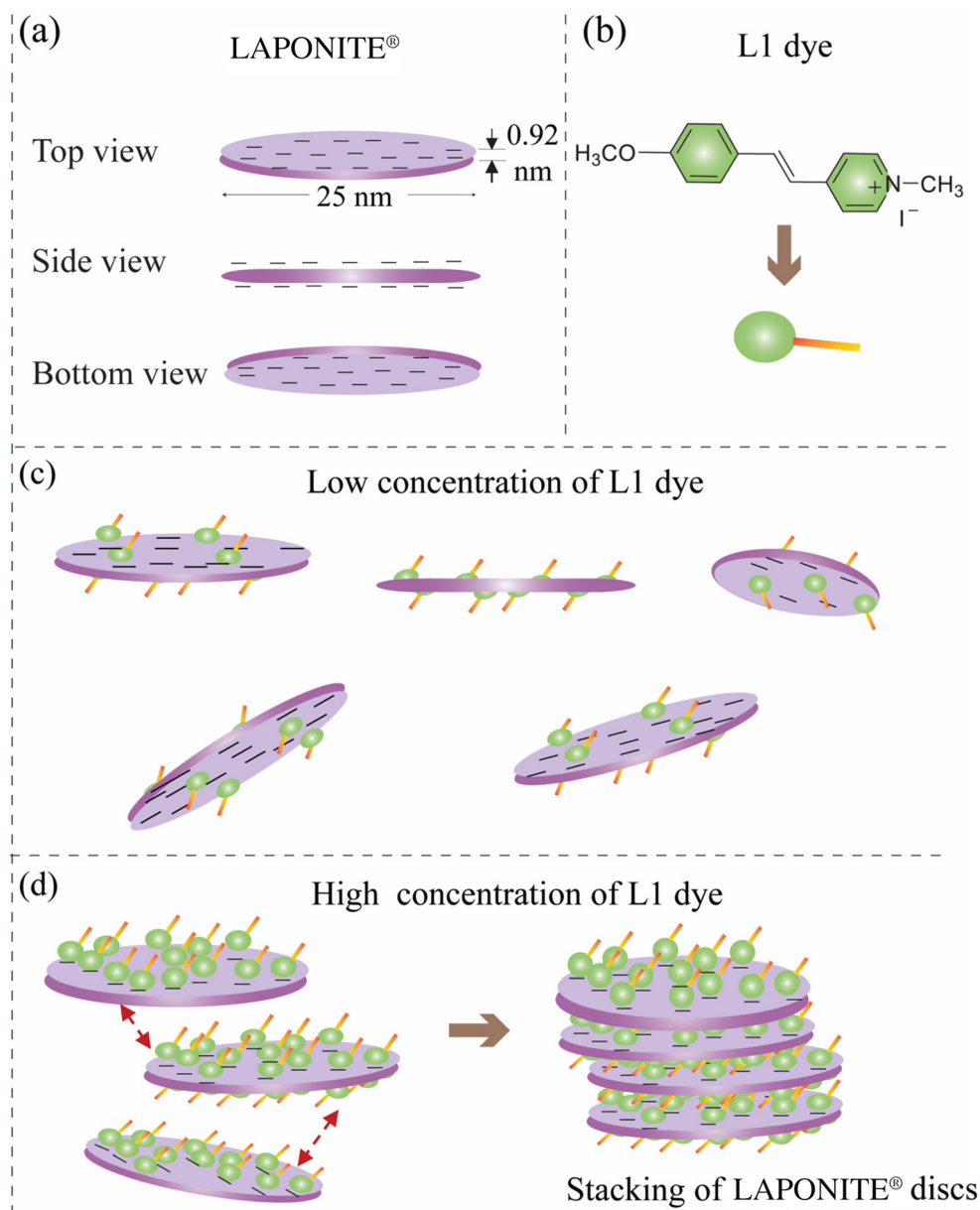
Fig. 1 Schematic illustration of the formation of large particles in a mixture of L1 dye/DMF + LAPONITE®/water. (a) Negatively charged LAPONITE® nano-discs in water; (b) molecular structure of L1 dye; (c) partially neutralized LAPONITE® nano-discs at a low concentration of dye; (d) stacking of surface-neutralized LAPONITE® nano-discs at a high concentration of dye.

transparent at a pump wavelength position of ~800 nm, while the linear absorption peak wavelength for the L1 dye solution in DMF is round 380 nm, revealing that the two-photon excitation wavelength should be around 800 nm.

Fig. 2(b) shows the comparison of the transmission spectra of two 1 cm samples: neat L1 dye/DMF of 0.02 M and the hybrid (mixture) solution (2 mL L1/DMF of 0.22 M + 0.2 mL LAPONITE®/water of 0.75 wt%), revealing that the scattering loss due to the LAPONITE® particles is ~5% around the pump wavelength range of ~800 nm.

3.   Results and discussion

3.1   Scattering behavior of neat dye/DMF, LAPONITE®/water, and hybrid solutions

Fig. 3(a) and (b) show photographs of the He–Ne laser beam scattering traces in different solutions with 1 cm path length. Fig. 3(a) indicates that the scattering strength is dependent on the LAPONITE® concentration but is comparable whether the solution is pure water or a mixture of DMF : water = 10 : 1. This indicates that the size and quantity of LAPONITE® clusters in
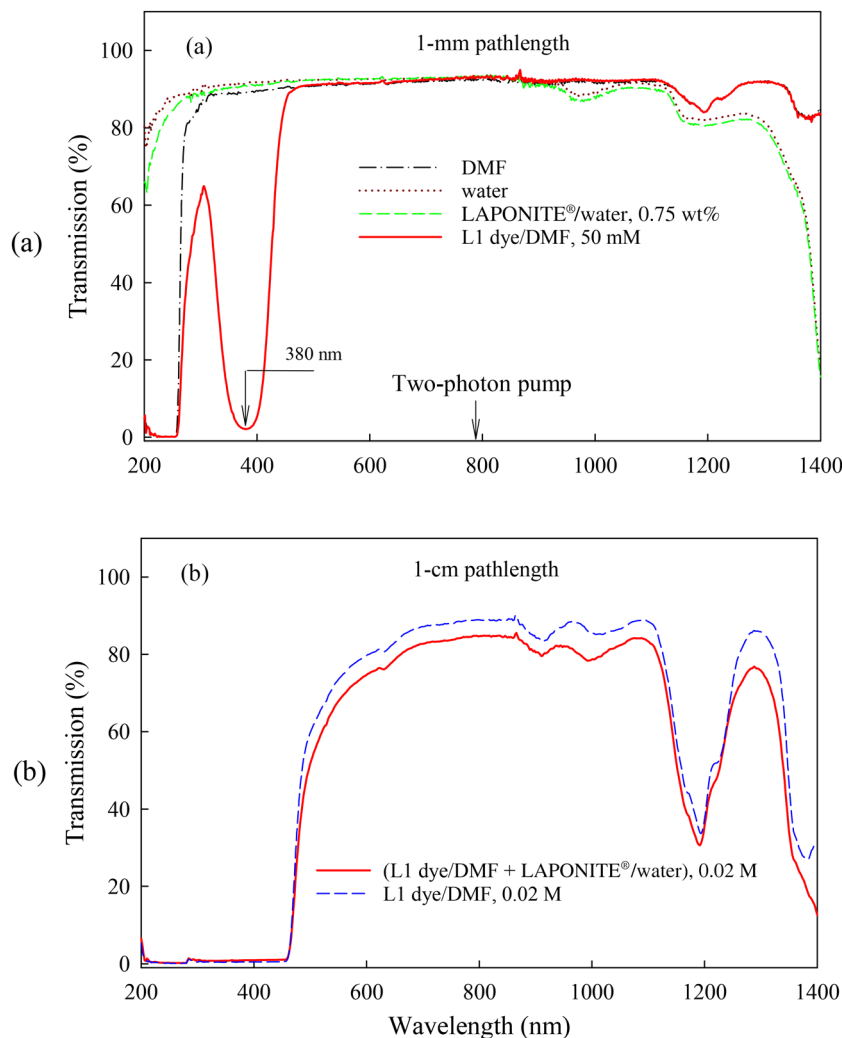
Fig. 2 Transmission spectra of (a) four 1 mm solution samples and (b) two 1 cm solution samples.

the examined formulations are not dependent on the amount of DMF. In contrast, when L1 is added to the LAPONITE® water/DMF solution, the scattering is much stronger. This reflects that the cationic exchange of L1 with LAPONITE®, and the subsequent reduction of electrostatic stabilization in solution, leads to increased agglomeration of the LAPONITE® nano-discs. Note that in Fig. 3(b), the scattering in the neat DMF dye solution is negligible, and the exposure time was longer than that in Fig. 3(a), showing the much weaker scattering in the neat dye solution.

Due to the 50-fold excess of L1 relative to the LAPONITE® exchange capacity in the solution, the amount of scattering can be tuned by increasing the LAPONITE® concentration 2–4 times. Fig. 3(c) and (d) exhibit the DLS measurements of LAPONITE® and the hybrid (mixture) solution, 10 : 1 (0.075 wt% LAPONITE®) and 10 : 2 (0.15 wt% LAPONITE®), respectively. The size of the LAPONITE® particles in these solutions ranges from ∼150 to ∼320 nm. The size of the aggregates does not increase with increasing LAPONITE® concen-

tration, rather the amount of aggregate increases, indicating that the size of the aggregates is primarily determined by the absorbed dye and solvent composition. Fig. 3(e) and (f) display the scanning electron microscopy images of LAPONITE® and the hybrid mixture, respectively, which clearly indicate the presence of larger size aggregates in the case of the hybrid mixture. It can be concluded that the scattering strength of LAPONITE® in pure water is dependent on its wt% value, and in the mixture of (L1/DMF + LAPONITE®/ water), the scattering strength is dependent on the size and number of the aggregated LAPONITE® particles.

3.2 Setup for regular and random lasing experiments

The experimental setup for the two-photon pumped lasing experiment is displayed in Fig. 4(a). A two-photon pump beam of 795 nm wavelength was generated from a 100 fs Ti:sapphire laser oscillator/amplifier system (Astrella HE, Coherent) operating at 100 Hz repetition rate. A pump beam of 4 mm diameter was focused by an $f = 15$ cm lens on the center of a 2 cm dia-
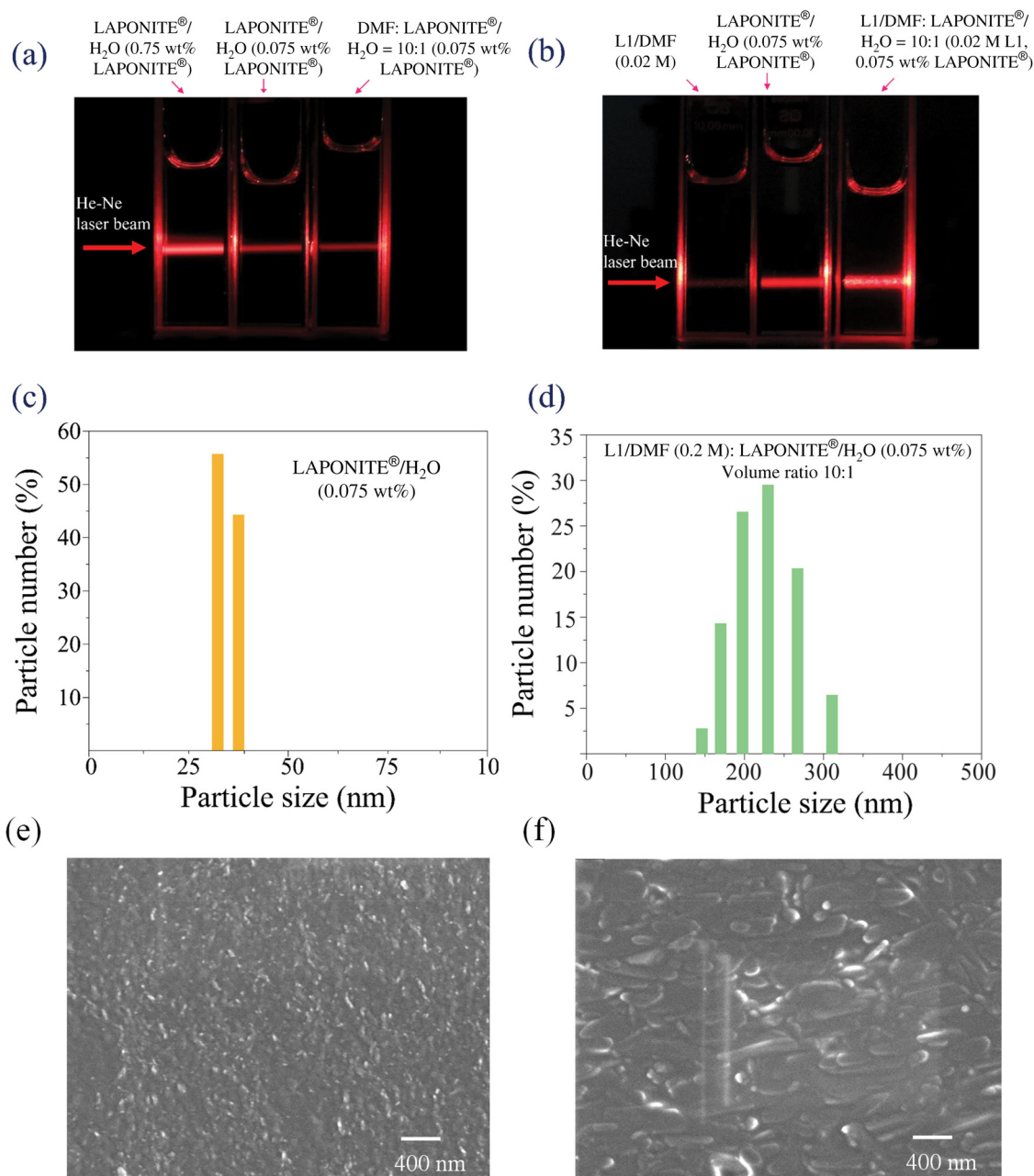
Fig. 3 He−Ne laser beam-induced scattering traces in (a) LAPONITE®/water and LAPONITE®/(water + DMF) solutions and (b) L1/DMF, LAPONITE®/water, and a mixture of L1 dye/DMF + LAPONITE®/water. Dynamic light scattering profiles of (c) LAPONITE®/water solution of 0.075 wt% and (d) a mixture of L1 dye/DMF10:1 (0.075 wt% LAPONITE®, 10 vol% H_2O). Scanning electron microscopy images based on (e) LAPONITE®/water solution of 0.075 wt% and (f) L1/DMF: LAPONITE®/water of volume ratio, 10:2 (0.15 wt% LAPONITE®).

meter glass vial (for random lasing measurement) or a 1 cm quartz cuvette (for lasing efficiency measurement).

The spectral curves of the emission signals along different directions were recorded using a grating spectrometer (HoLo Spec, Kaiser Optical Systems) in conjunction with a fiber coupler of ~1 mm acceptance diameter; the resolution of this spectrometer was ~1.5 nm in the working range of 400–823 nm.

The temporal behavior of two-photon pumped regular lasing and random lasing were measured using a streak camera (C-5680-22, Hamamatsu) with a temporal solution of ~2 ps when working in the 0.2 ns scanning range.

Under our experimental conditions of a 2 cm sample of L1 dye in the hybrid solution (2 mL L1/DMF of 0.22 M + 0.2 mL LAPONITE®/water of 0.75 wt%), the additional scattering loss due to the large-size LAPONITE® particles is about 10% (see Fig. 2(b)), so that most of the pump energy remains propagated along the forward directions to generate forward and backward regular lasing. In the meantime, stimulated emis-
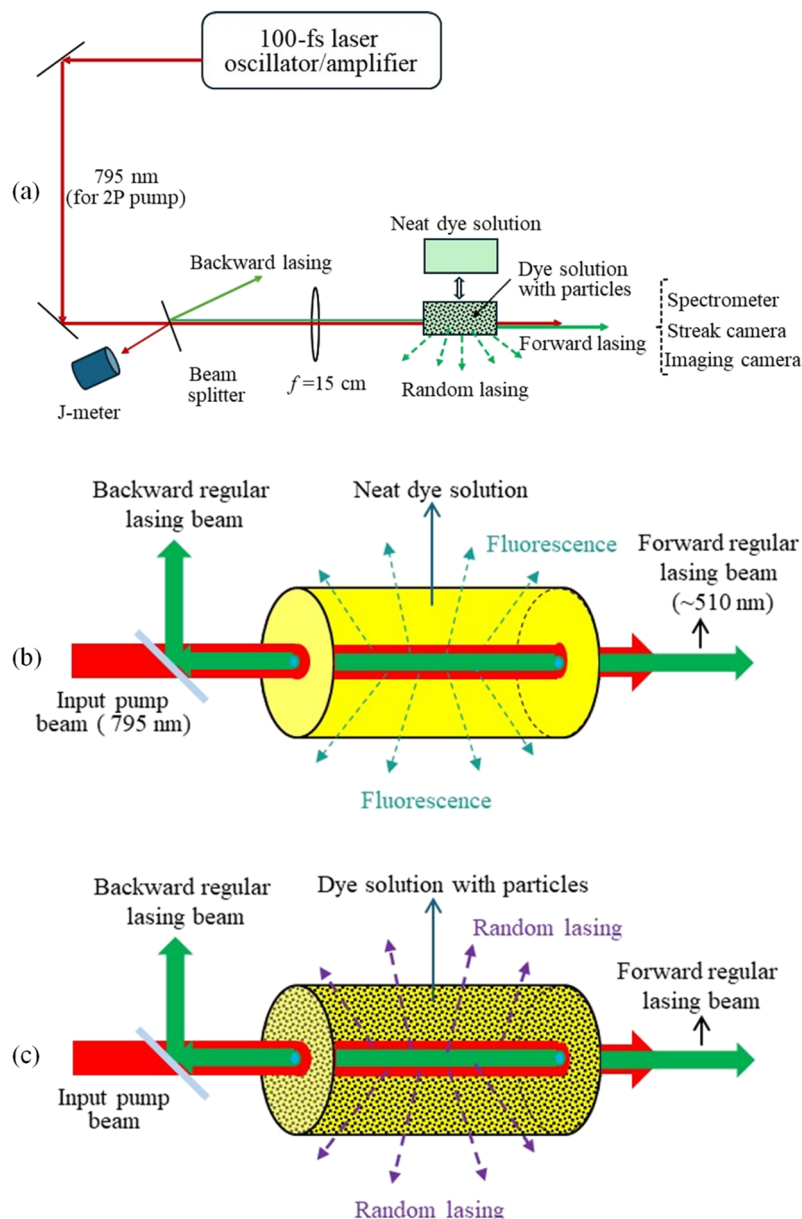
Fig. 4 (a) Optical set-up for the two-photon pumped lasing experiment; (b) schematic illustration of regular lasing in a neat dye solution sample; and (c) schematic illustration of regular and random lasing in a scattering dye solution sample.

sion along all other directions may also be created by the ~10% scattered pump energy provided that the input pump energy level is high enough. This means that the pump energy threshold for random lasing should be much higher than that for forward regular lasing. This prediction is proved by our measured results described later in section 3.4.

3.3 Spectral behaviors of two-photon pumped regular and random lasing

Based on the experimental configuration schematically shown in Fig. 4(a), once the input pump pulse is higher than a certain threshold value, highly directional regular lasing can be generated in both forward and backward directions in the

neat L1 dye/DMF solution sample of 0.02 M concentration and 2 cm path length, while we can also see the fluorescence emission in all other directions as schematically shown in Fig. 4(b). Considering upon excitation with a 100 fs pump pulse that dye population inversion can only exist for a period shorter than several tenths of picoseconds,[2,3] even for a cavity of ~1 cm length, the cavity round time (~100 ps) will be much longer than the population inversion retaining time, so that multi-pass lasing across the cavity is not achievable. However, by using a focused pump beam, only the initial stimulated emission signals propagating along the forward and backward directions can obtain the maximum gain length. In contrast, the initial stimulated emission signals propagating along the

directions far apart from the pump beam direction do not acquire enough gain length and still retain their spontaneous emission nature.

As schematically shown in Fig. 4(c), under the same experimental conditions, after replacing the neat dye solution with a solution mixture of the same dye concentration but containing large-size (200–300 nm) LAPONITE® particles of 0.075 wt% concentration, we could observe both regular lasing along the forward/backward directions and random lasing along all other directions. In this case, the random lasing signals are characterized by their spectral narrowing and pump threshold requirement. Under our experimental conditions, the generation of random lasing is based on the following two facts: (i) partial forward pump energy is redistributed by particle scattering, providing a gain potential along all directions and (ii) partial energy

of strong forward lasing is also scattered into all directions, providing a seed stimulated signal. Due to these two reasons, spatially random lasing signals could be observed with a pump threshold higher than that for forward lasing generation.

Fig. 5(a) shows the spectral curves measured in the neat dye solution (filled in a vertically placed glass vial of 2 cm diameter) along different directions indicated in the upper-right corner inset. The input energy of the 795 nm laser pulse was 47 μJ. From this figure, we can clearly see that the width of the spectral peak for both the forward and backward lasing outputs is significantly narrower than the spontaneous fluorescence spectral peaks, which can be observed along all other directions.

Fig. 5(b) shows the spectral curves measured in the mixture (hybrid) solution (filled in the same glass vial) along different
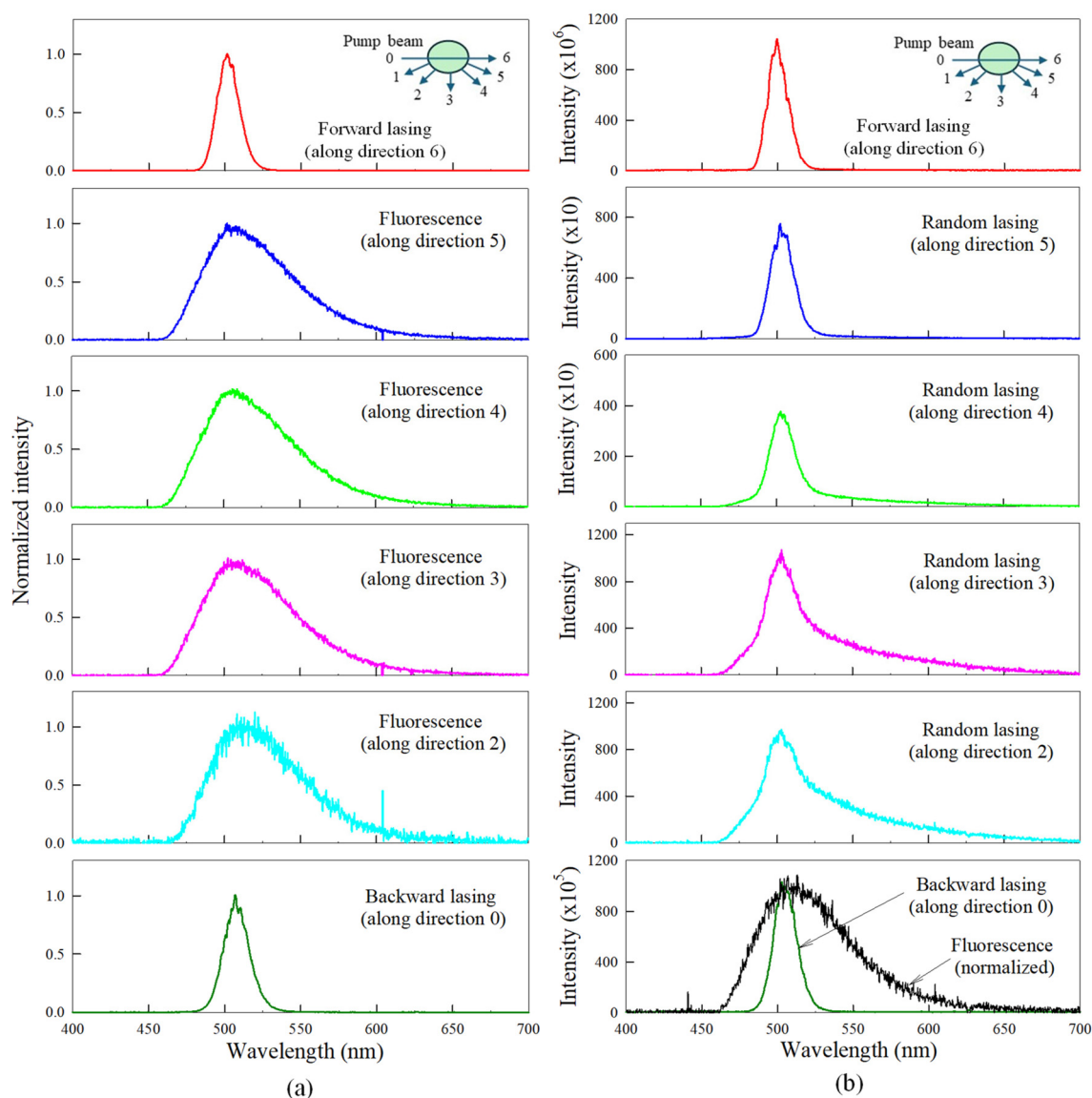

Fig. 5 (a) Two-photon pumped regular lasing and fluorescence spectra from a 2 cm glass vial filled with neat L1 dye/DMF; (b) two-photon pumped regular and random lasing spectra from a 2 cm glass vial filled with a mixture of L1 dye/DMF + LAPONITE®/water. Pump energy: ~47 μJ; exposure time: 50 ms.

directions and under the same pump energy level of 47 μJ. Regular forward lasing and backward lasing remain highly directional, whereas random lasing can be detected along all other directions. The detecting fiber coupler of ~1 mm aperture was kept at a 4 mm distance from the wall of the glass vial. Here, the relative spectral intensity detected by the fiber coupler represents the relative spectral brightness, *i.e.* the light power/[cm^2(area)·sr (acceptance solid angle)·nm(spectral interval)]. Since the spectral brightness of forward and backward lasing is many orders of magnitude higher than random lasing, high-attenuation neutral filters were placed in front of the fiber coupler when the forward and backward lasing outputs were measured. The backward lasing beam was reflected by a beam splitter and re-entered into the fiber coupler *via* another focused lens. Random lasing along directions 2 and 3 reveals a central narrowed peak accompanied by two broad spectral wings, whereas random lasing along directions 4 and 5 reveals basically the same spectral profiles as the regular lasing output. The peak spectral brightness ratio between traditional forward lasing and random lasing is in the range of $10^5 : 1$–$10^6 : 1$. The ratio between forward and backward lasing is about $10 : 1$.

3.4 Evolution of random lasing and comparison with fluorescence emission

Fig. 6 shows the spectral profiles of the random lasing signals as a function of the pump energy measured along direction 4. When the mixture sample was pumped at a low energy level (<10 μJ), the recorded spectral curve is like the fluorescence profile from the neat L1/DMF dye solution. At moderate pump levels (15–30 μJ), spectral narrowing begins to appear, and at high pump levels (40–50 μJ), nearly completed spectral narrowing can be achieved. Based on these measurements, the pump energy threshold for random lasing can be roughly estimated as ~30 μJ (corresponding to the pump fluence at a focal position of ~171 mJ cm^{-2}); this value is remarkably higher than the threshold value for generating forward lasing from the same solution, which is about 2–3 μJ (corresponding to 11.4–17.1 mJ cm^{-2} at the focal position).

Fig. 7 shows the spectral curve measured in the mixture sample along direction 4 in comparison with the fluorescence spectral curve measured in the neat dye solution sample under the same conditions of pump energy (47 μJ) and exposure time (50 ms). Based on the comparison of these two spectral profiles, we know that the peak spectral intensity (brightness) ratio between random lasing and fluorescence emission at the wavelength position pf ~500 nm is about 3.3 : 1. However, the ratio of areas covered by these two spectral profiles is 1.07 : 1, which means that the spectral energy of these two emission signals are nearly the same.

3.5 Temporal behaviors of two-photon pumped lasing pulses

The temporal behavior of two-photon pumped lasing from the neat L1 dye/DMF and from the hybrid mixture (L1 dye/DMF + LAPONITE®/water) was measured separately using a streak camera working in the 200 ps scanning range with a resolution of ~2 ps.
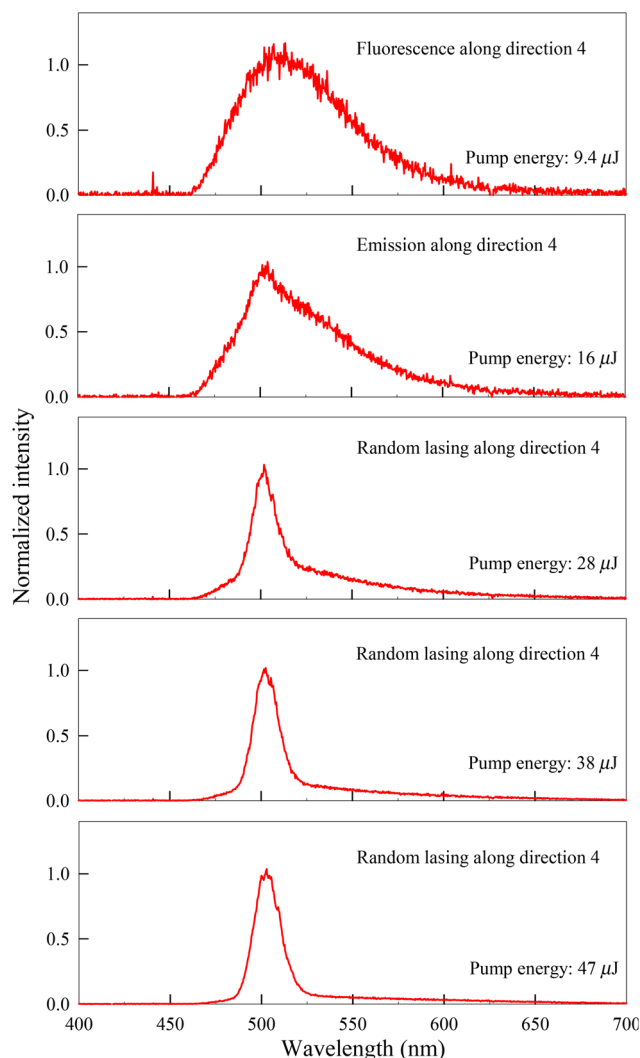

Fig. 6 Growth of two-photon pumped random lasing of L1 dye/DMF + LAPONITE®/water with increasing pump energy; exposure time: 50 ms.

Fig. 8(a) shows the temporal waveforms of the transmitted pump pulse and the forward lasing pulse from the neat dye solution, wherein the transmitted pump pulse was strongly attenuated using spectral filters. There is an apparent time delay of 6.2 ps between the pump pulse peak and the forward lasing peak. Owing to the group-velocity-dispersion effect of the optical elements inside the camera system with respect to the wavelength difference between the pump light (~800 nm) and the lasing light (~500 nm), the inherent time delay of these two pulses is ~2 ps; therefore, the real-time delay between these two incident pulses should be ~4 ps, which reflects the build-up time of population inversion in the emission state of the dye molecules. Fig. 8(b) shows the exponential decay of fluorescence emission from the same solution, but excited with an unfocused pump beam. Comparing (a) to (b) indicates that forward lasing can last only ~10 ps, whereas the fluorescence life-time is ~75 ps.
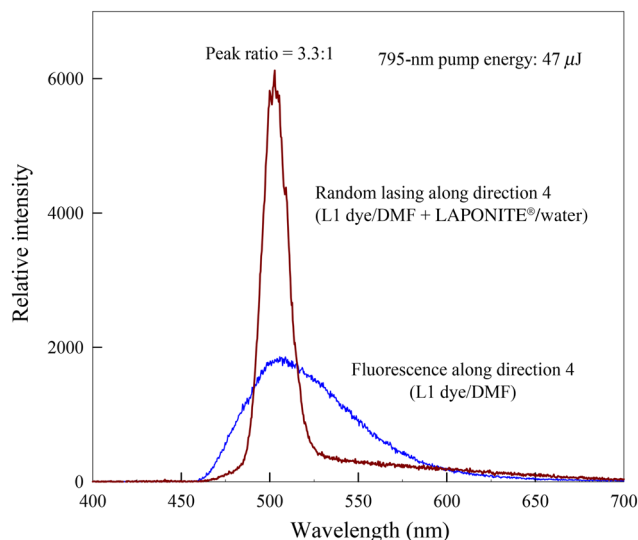
Fig. 7 Comparison between the spectral profiles of random lasing from L1 dye/DMF + LAPONITE®/water and the fluorescence emission from L1 dye/DMF.

Fig. 8(c) shows the temporal waveforms of the pump pulse and forward lasing pulse from the hybrid solution. Here, the real-time delay between the transmitted pump pulse and the

lasing pulse is ~5.4 ps, while the forward lasing duration time is ~7 ps. Meanwhile, the waveform of the random lasing pulse measured along direction 3 is shown in Fig. 8(d), indicating that the emission peak lasts ~15 ps with a slowly decaying tail. The different temporal behaviors between forward lasing and random lasing can be tentatively interpreted as follows: the former, colinearly traveling with the pump pulse, together may preferentially exhaust most of the population inversion to obtain maximum amplification within a relatively short period of time, whereas random lasing along a side direction exhibits much shorter gain length and therefore can only take place based on the leftover population inversion not yet entirely exhausted by the forward lasing pulse.

3.6 Near- and far-field patterns of regular lasing beams

Fig. 9(a) shows the near-field and far-field patterns of the 795 nm pump beam; here, the near-field pattern was the section image of the unfocused pump beam, while the far-field pattern was the focal spot image of the pump beam focused by an f = 40 cm lens. This figure indicates that the input pump beam size was ~4 mm, and the beam divergence angle was ~1 mrad.

Fig. 9(b) shows the near- and far-field patterns of the regular forward and backward lasing beams from the neat L1/DMF solution of 0.02 M. Here, the near-field patterns were the section images of the recollimated output lasing beams *via* an
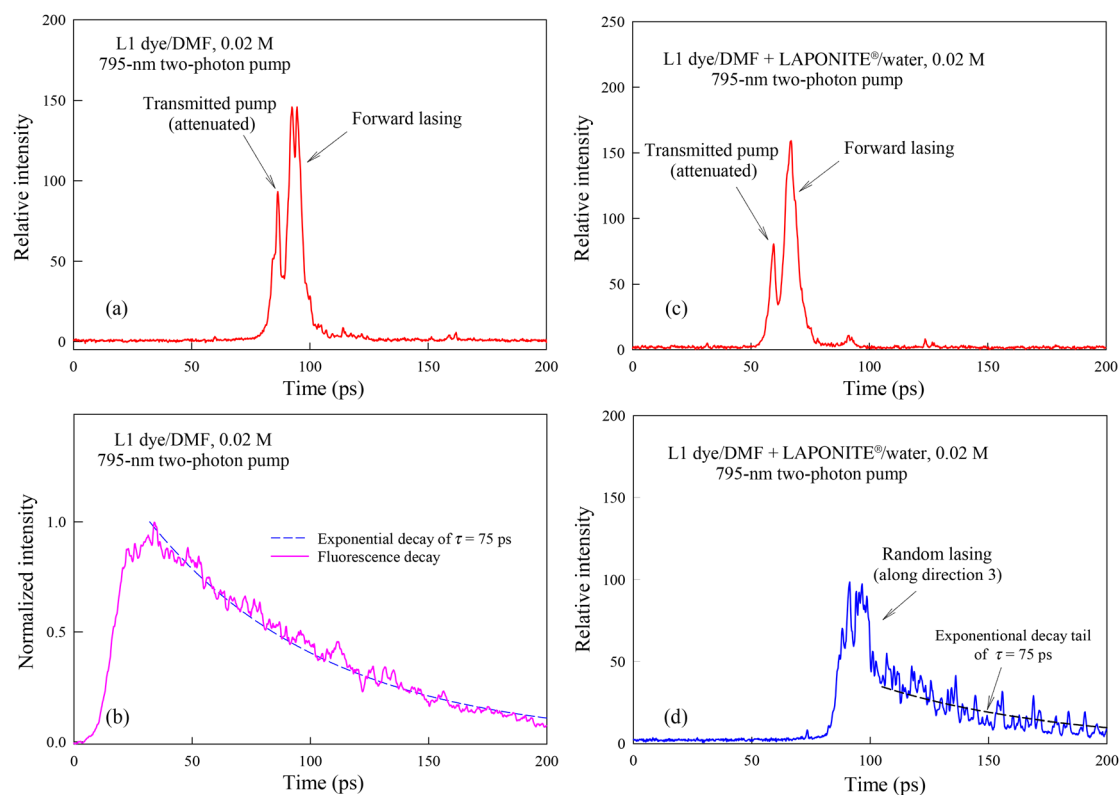

Fig. 8 Temporal waveforms of (a) traditional forward lasing and (b) the fluorescence emission from the neat dye solution. Temporal waveforms of (c) traditional forward lasing and (d) random lasing along direction 3 from a hybrid solution. The relative position of the spectral curve along the time axis is arbitrary. Pump pulse energy: ~47 μJ; exposure time: 20 ms.

Near-field pattern (parallel beam) — 5 mm

Far-field pattern (focused beam) — 1 mm

Pump beam

(a)

Near-field — 5 mm

Far-field — 1 mm

Forward lasing

Near-field — 5 mm

Far-field — 1 mm

Forward lasing

Backward lasing — 5 mm / 1 mm

Backward lasing — 5 mm / 1 mm

Regular lasing beam from neat L1 dye/DMF

(b)

Regular lasing beam from L1 dye/DMF + LAPONITE®/water)

(c)

Near-field pattern of backward lasing beam

Focusing lens

Dye solution

Near-field pattern of forward lasing beam

Far-field pattern

Pump beam

Beam splitter

Collimating lens

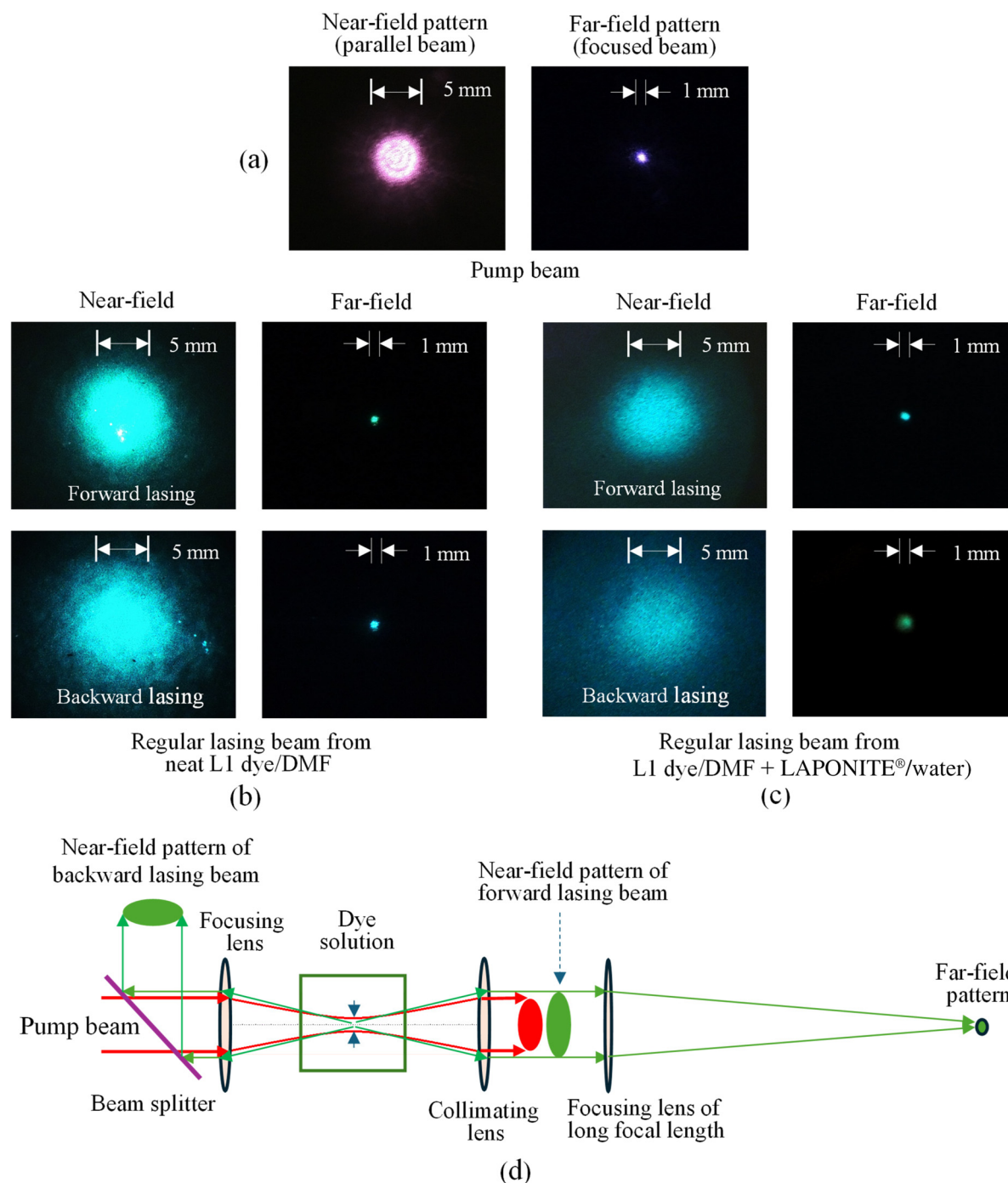Focusing lens of long focal length

(d)

Fig. 9 Near- and far-field patterns of (a) 795 nm pump beam, (b) two-photon pumped forward and backward lasing beams from a neat L1 dye/DMF solution, (c) two-photon pumped forward and backward lasing beams from a dye–LAPONITE® hybrid solution, and (d) schematic illustration of the near- and far-field pattern sampling.

f = 15 cm lens, while the far-field patterns were recorded by refocusing these beams by the same f = 40 cm lens. In these cases, the divergence angles of the forward and backward lasing beams were basically the same as the input pump beam. This is reasonable as the divergence angle of the lasing beam is determined by the focal spot size of the input pump beam in the center of the gain medium. In contrast, the sizes of the recollimated lasing beams were slightly larger than the pump beam due to the following reason: within the high gain region determined by the pump focal geometry, there is a certain tolerance allowing these stimulated emission components to be slightly deviated from the pump beam propagation direction and thus they can also be lasing (see Fig. 9(d)).

Fig. 9(c) shows the near- and far-field patterns of the forward and backward lasing beams from the dye–LAPONITE® hybrid solution. In comparison with Fig. 9(b), we can see that the borders of the near- and far-field patterns of the lasing beams from the hybrid sample seem more diffused than those of the lasing beams from the neat solution, which is due to the scattering influences from the LAPONITE® particles.

Finally, Fig. 9(d) presents a schematic illustration of the near- and far-field pattern sampling.

3.7 Output/input relationships under two-photon pump conditions

Fig. 10 shows the output/input curves measured in a neat L1/DMF solution of 0.02 M and in three hybrid solutions of the same dye concentration but with different LAPONITE® particle concentrations. The lasing threshold becomes higher by increasing the concentration of the LAPONITE® particles, while the lasing efficiency defined as the ratio of output lasing energy to input pump energy becomes lower. At a pump energy level of ~22.5 μJ, the measured lasing efficiency for the 4 solutions is 9.9%, 8.4%, 6.8% and 4%, respectively. These variations in the lasing efficiency can be explained by considering the different influences of scattering losses on lasing generation.

In our case, with an increase in LAPONITE® concentration, a greater scattering loss of the input pump beam leads to a lower efficiency of regular lasing. Even so, we could still generate lasing along both the forward/backward directions and random lasing along all other directions, as the scattering losses here are still within a controllable range (e.g. ≤10–20%).
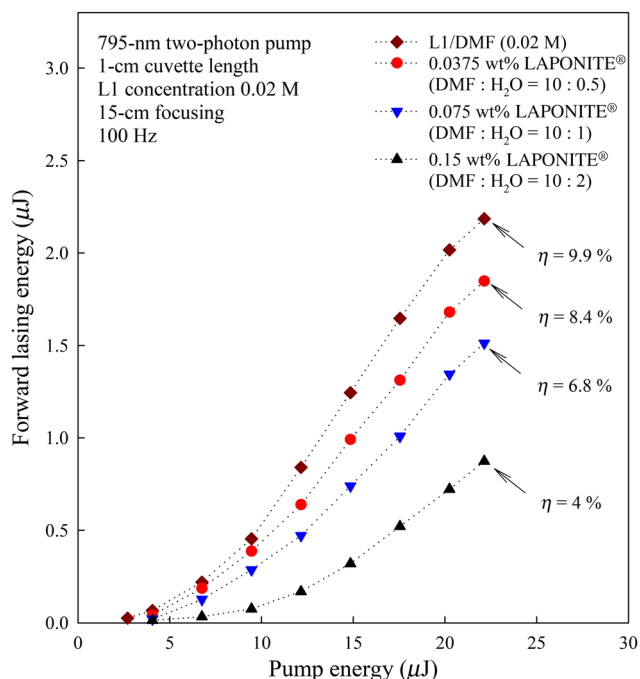
However, in most experiments of random lasing studies,[15–21] the scattering actions of the gain media were so strong that no directional lasing could be generated.

4. Conclusion

Two-photon pumped regular and random lasing has been generated in a stilbazolium dye solution containing large-size LAPONITE® nanoparticles as scattering centers. Traditional forward/backward lasing is characterized by high directionality, high spectral brightness, and spectral and temporal narrowing, whereas random lasing is characterized only by spectral and temporal narrowing. We have elucidated that the spatial, temporal, and threshold behaviors of traditional lasing and random lasing are different. The measured spectral brightness for forward lasing is 10^5–10^6 times higher than that for random lasing. On the other hand, under the same input pump conditions, the peak spectral intensity of random lasing from the hybrid solution is 3.4 times higher than that of the fluorescence emission from the neat dye solution, but the energy for the two emission signals is the same. This study demonstrates that both multi-photon pumped traditional and random lasing can be generated in a moderately scattering gain medium.

Data availability

The data will be made available by the authors upon reasonable request.

Conflicts of interest

The authors declare no conflict of interest.

Acknowledgements

References

1 G. S. He, L.-S. Tan, Q. Zheng and P. N. Prasad, *Chem. Rev.*, 2008, **108**, 1245–1330.
2 G. S. He, P. P. Markowicz, T. C. Lin and P. N. Prasad, *Nature*, 2002, **415**, 767–770.
3 G. S. He, T.-C. Lin, S.-J. Chung, Q. Zheng, C. Lu, Y. Cui and P. N. Prasad, *J. Opt. Soc. Am. B*, 2005, **22**, 2219–2228.
4 Q. Zheng, H. Zhu, S.-C. Chen, C. Tang, E. Ma and X. Chen, *Nat. Photonics*, 2013, **7**, 234–239.

Fig. 10 Two-photon pump forward lasing output from four solutions of different particle concentrations *versus* input pump energy.

5 H. Zhu, A. Chen, Y. Wu, W. F. Zhang, S. Su, X. Ji, P. T. Jing, S.-F. Yu, C. Shan and F. Huang, *Adv. Opt. Mater.*, 2018, **6**, 1800518.

6 Y. Jiang, K. F. Li, K. Gao, H. Lin, H. L. Tam, Y. Y. Liu, Y. Shu, K. L. Wong, W. Y. Lai, K. W. Cheah and W. Huang, *Angew. Chem., Int. Ed.*, 2021, **60**, 10007–10015.

7 X. Wang, H. Zhou, S. Yuan, W. Zheng, Y. Jiang, X. Zhuang, H. Liu, Q. Zhang, X. Zhu, X. Wang and A. Pan, *Nano Res.*, 2017, **10**, 3385–3395.

8 M. Li, M. Zhi, H. Zhu, W.-Y. Wu, Q.-H. Xu, M. H. Jhon and Y. Chan, *Nat. Commun.*, 2015, **6**, 8513.

9 J. Yu, Y. Cui, H. Xu, Y. Yang, Z. Wang, B. Chen and G. Qian, *Nat. Commun.*, 2013, **4**, 2719.

10 C. Zhang, F. Zhang, T. Zhu, A. Cheng, J. Xu, Q. Zhang, S. E. Mohney, R. H. Henderson and Y. A. Wang, *Opt. Lett.*, 2008, **33**, 2437–2439.

11 G. Xing, Y. Liao, X. Wu, S. Chakrabortty, X. Liu, E. K. Yeow, Y. Chan and T. C. Sum, *ACS Nano*, 2012, **6**, 10835–10844.

12 M. Kazes, D. Y. Lewis, Y. Ebenstein, T. Mokari and U. Banin, *Adv. Mater.*, 2002, **14**, 317–321.

13 G. Tsiminis, A. Ruseckas, I. D. W. Samuel and G. A. Turnbull, *Appl. Phys. Lett.*, 2009, **94**, 253304.

14 F. Scotognella, D. P. Puzzo, M. Zavelani-Rossi, J. Clark, M. Sebastian, G. A. Ozin and G. Lanzani, *Chem. Mater.*, 2011, **23**, 805–809.

15 N. M. Lawandy, R. M. Balachandran, A. S. L. Gomes and E. Sauvain, *Nature*, 1994, **368**, 436–438.

16 A. S. L. Gomes, M. T. Carvalho, C. T. Dominguez, C. B. de Araújo and P. N. Prasad, *Opt. Express*, 2014, **22**, 14305–14310.

17 Z. Shang, M. Yang and L. Deng, *Materials*, 2016, **9**, 725.

18 J. Kitur, G. Zhu, M. Bahoura and M. A. Noginov, *J. Opt.*, 2010, **12**, 024009.

19 M. Leonetti, C. Conti and C. Lopez, *Nat. Photonics*, 2011, **5**, 615–617.

20 J. Azkargorta, I. Iparraguirre, M. Barredo-Zuriarrain, S. García-Revilla, R. Balda and J. Fernández, *Materials*, 2016, **9**, 369.

21 A. Consoli, D. Mariano da Silva, N. U. Wetter and C. López, *Opt. Express*, 2015, **23**, 29954–29963.

22 K. Neeraj and M. Chandra, in *Clay and Clay Minerals*, ed. N. Gustavo Morari Do, IntechOpen, Rijeka, Ch. 2, 2021, DOI: **10.5772/intechopen.97672**.

23 N. Padiyakkuth, S. Thomas, R. Antoine and N. Kalarikkal, *Mater. Adv.*, 2022, **3**, 6687–6706.

24 K. Lupinska, M. Durko-Maciag, C. Andraud, Y. Bretonnière, P. Hanczyc, P. Fita, P. Szulim, J. Mysliwiec and L. Sznitko, *J. Mater. Chem. C*, 2023, **11**, 4937–4945.

25 Y. Zhang, Q. Zhang and X. Zhang, *Opt. Commun.*, 2024, **569**, 130814.

26 V. Martínez Martínez, F. López Arbeloa, J. Bañuelos Prieto, T. Arbeloa López and I. López Arbeloa, *Langmuir*, 2004, **20**, 5709–5717.

27 N. Padiyakkuth, R. Antoine and N. Kalarikkal, *Opt. Mater.*, 2022, **129**, 112408.

28 A. Pramanik, A. Sciortino, M. Reale, P. Pasbakhsh, G. Cavallaro, M. Cannas, G. Lazzara and F. Messina, *ACS Appl. Nano Mater.*, 2023, **6**, 15896–15905.

29 H. v. Olphen, *An Introduction to Clay Colloid Chemistry*, Wiley, 1977.

30 X. Tan, F. Liu, L. Hu, A. H. Reed, Y. Furukawa and G. Zhang, *Appl. Clay Sci.*, 2017, **135**, 313–324.

31 K. Suman and Y. M. Joshi, *Langmuir*, 2018, **34**, 13079–13103.

32 S. Gupta, G. S. He, V. Kumar, A. Pitter, M. Trebbin, M. T. Swihart, R. K. Kumar, L. Nebhani, Y. M. Joshi, R. A. Vaia and P. N. Prasad, *J. Phys. Chem. C*, 2024, **128**, 17961–17970.